Available online at www.sciencedirect.com
ScienceDirect
International Journal of Mass Spectrometry 261 (2007) 192–198
International Journal of Mass Spectrometry
www.elsevier.com/locate/ijms

# Aspirin revealed: A cationization strategy for detecting acetylsalicylic acid by MALDI mass spectrometry

D. Lacey [a], X.K. Hu [a], A.V. Loboda [b], N.J. Mosey [a], R.H. Lipson [a,*]

[a] *Department of Chemistry, University of Western Ontario, London, Ont. N6A 5B7, Canada*
[b] *MDS SCIEX, 71 Four Valley Drive, Concord, Ont. L4K 2V8, Canada*

Received 16 June 2006; received in revised form 8 September 2006; accepted 10 September 2006
Available online 10 October 2006

**Abstract**

Experiments are described where the experimental conditions have been optimized to detect aspirin by MALDI mass spectrometry. Although protonated aspirin was not observed by MALDI, sodium and potassium aspirin adducts could be found. Significantly better signals could be obtained by using Rb and Cs salts as cationization sources. Quantum calculations were carried out to determine the structure and energetics of the Li, K, Rb, and Cs alkali—aspirin adducts.


*Keywords:* MALDI; Aspirin; Cationization; Structure

## 1. Introduction

Aspirin (acetylsalicylic acid or ASA) is arguably the world's oldest and best known pharmaceutical product with accepted anti-inflammatory, anti-thrombotic, anti-pyretic, anti-oxidant and analgesic properties [1,2]. It has been suggested that daily use of aspirin can reduce the risk of some types of cancer [3], and even provide a means of extending human life span [4]. At the same time, it is estimated that 8–45% of the population are actually aspirin-resistant [5]. It is therefore not surprising that a number of analytical techniques have been developed to detect aspirin directly or in human plasma. These include desorption electrospray ionization (DESI) mass spectrometry (MS) [6], atmospheric pressure chemical ionization (APCI)-MS [7], and gas chromatography (GC)–tandem MS [8]. Low-level determination of this compound is also possible by high performance liquid chromatography (HPLC) [9]. Surprisingly, however, there have been no reports on the use of matrix assisted laser desorption ionization (MALDI)-MS [10] to detect this important drug.

Despite misconceptions to the opposite, MALDI MS is actually emerging as a powerful tool for small drug analysis [11] in part because unlike ESI-MS, MALDI signals are not prone to suppression by salts or buffers in the sample. However, the difficulties associated with small molecule detection by MALDI-MS are also well known. The most obvious one is the potential for isobaric interferences from the matrix itself. Small molecules also tend to be less readily ionizable due to a paucity of polar groups, and their increased volatility can lead to sample loss during preparation and in the vacuum chamber of the mass spectrometer.

A number of solutions have been proposed that circumvent these issues. One involves chemically derivatizing the drug molecules to reduce their volatility and to shift their masses into a range outside that of the matrix [12]. Another has been to add surfactants to the sample to suppress the matrix-related ion background [13]. One very promising innovation is the use of a high repetition rate laser (kHz versus 10s of Hz) to record MALDI spectra [14–17]. Here, the ability to accumulate a larger number of spectra in a shorter time can improve the ion signal intensity reproducibility (a severe problem associated with MALDI) and allow a higher sample throughput. In many of these studies the MALDI source was interfaced to a triple quadrupole (QqQ) mass spectrometer instead of the more common time-of-flight instrument. In its simplest configuration a triple quadrupole mass spectrometer can act as a mass filter for the analyte ion of interest.

In this work conventional ultraviolet (UV)-MALDI (20 Hz repetition rate) experiments using a triple quadrupole mass

* Corresponding author. Tel.: +1 519 661 2111; fax: +1 519 661 3022.
*E-mail address:* rlipson@uwo.ca (R.H. Lipson).

1387-3806/$ – see front matter © 2006 Elsevier B.V. All rights reserved.
doi:10.1016/j.ijms.2006.09.022

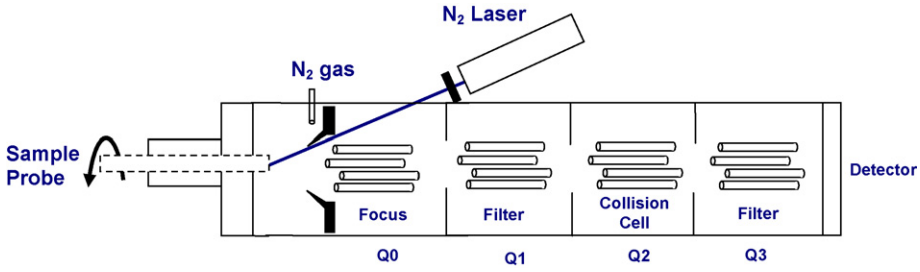


Fig. 1. Schematic of the experimental apparatus used to record UV-MALDI mass spectra of aspirin.

spectrometer were carried out to determine the limitations of aspirin detection by MALDI-MS. It was found that MALDI MS can be used to detect aspirin but with reduced sensitivity compared to other analytes. The addition of salts to the matrix, however, enhances the probability of aspirin detection. Insight into this effect was explored by calculating the structures and energetics of the observed adduct ions.

## 2. Experimental/materials and methods

The experimental apparatus used to record UV-MALDI mass spectra of aspirin is shown schematically in Fig. 1. Ultraviolet (UV) pulses from a $N_2$ laser (Thermo Laser Science, model VSL-337ND-S) at $\lambda = 337$ nm, each with ~50 μJ energy in 10 ns, were introduced at a 20 Hz repetition rate by optical fiber into the ionization region of a MALDI mass spectrometer. The laser pulses were focused to an ~0.063 $mm^2$ area spot size with an $f = 10$ cm lens onto the surface of a 1.0 cm diameter sample plate, which was continuously rotated at a speed of 0.4 rpm. The laser intensity at the output of the optical fiber was measured with a power meter (Ophir Electronics, model NOVA).

The prototype MALDI instrument was built by replacing the front end of an Applied Biosystems/MDS Sciex API-365 LC/MS/MS triple quadrupole (QqQ) mass spectrometer originally configured for electrospray ionization with a home-made MALDI ion source. All spectra were obtained by scanning the first quadrupole ($Q_1$). The instrument was operated in positive ion mode. MALDI cations were detected with a channeltron electron multiplier (Burle Industries).

The triple quadrupole mass spectrometer was maintained at a pressure of ~$10^{-5}$ Torr by two turbo pumps connected in parallel and backed by a mechanical pump. During the experiments, 0.1 Torr of $N_2$ gas was introduced into the ionization region of the spectrometer to cool the ions and improve the ion focusing.

Aspirin, >99% purity, and 2,5-dihydroxybenzoic acid (DHB) matrix, >98% purity were purchased from Aldrich and used without further purification. A majority of the samples were prepared using the sandwich technique [18]. Evidence of a weak matrix suppression effect (MSE) [19] was seen by studying samples with different DHB to ASA ratios. Concentration studies showed that DHB:ASA molar ratios between 4 and 6 were most advantageous in this regard.

In some of the experiments sodium trifluoroacetic acid (Aldrich; >98% purity), and the alkali chloride salts (LiCl, KCl, RbCl, and CsCl) (Aldrich; >99% purity) were used as matrix additives.

## 3. Results

Portions of a typical MALDI spectrum of ASA in DHB between $m/z = 200$ and 400 is shown in Fig. 2. No peaks thought to be associated with ASA were found above $m/z = 400$. Table 1 lists the peaks present in the ASA/DHB MALDI spectrum that

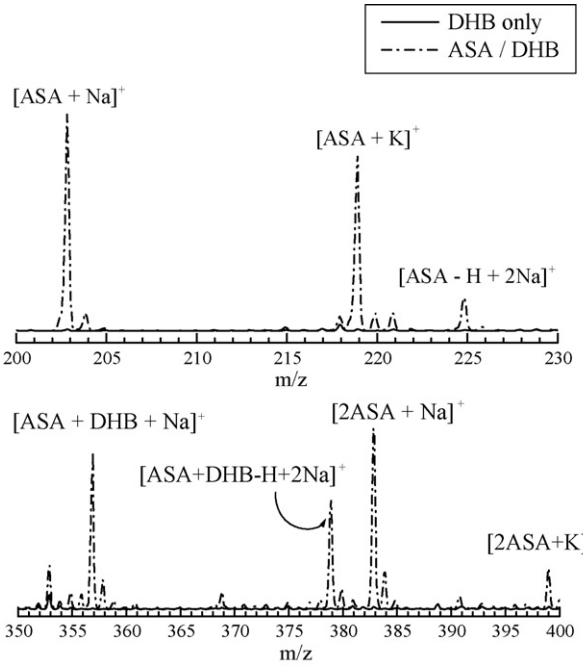


Fig. 2. Portions of the MALDI mass spectrum of aspirin in a DHB matrix showing aspirin-related peaks superimposed on the MALDI mass spectrum of DHB alone over the same $m/z$ ranges.

Table 1
Peaks seen in the MALDI-MS of aspirin in DHB that were not observed in the spectrum for DHB only, and their proposed formulae

| $m/z$ | Proposed formula |
|---|---|
| 203 | $(ASA + Na)^+$ |
| 219 | $(ASA + K)^+$ |
| 225 | $(ASA - H + 2Na)^+$ |
| 357 | $(ASA + DHB + Na)^+$ |
| 379 | $(ASA + DHB - H + 2Na)^+$ |
| 383 | $(2ASA + Na)^+$ |
| 399 | $(2ASA + K)^+$ |

were not found in the DHB spectrum alone, along with the proposed formula for each peak. The signals in the mass spectrum were normalized such that the largest peak in the spectrum (a feature associated with the MALDI spectrum of DHB alone) was assigned an intensity of unity. Signals due to aspirin or protonated aspirin were not observed. Similarly, preliminary spectra run in negative ion mode showed no features that could be attributed to aspirin. Instead, all aspirin-related signals were either complexes of the molecule with one Na or one K ion, or the deprotonated species complexed to two alkali metals. Presumably, the alkali metal ions are impurities which are ubiquitous in these systems unless care is taken to remove them. Additional features in the spectrum could be assigned to a heterocluster of ASA + DHB complexed to $Na^+$, a deprotonated ASB-DHB cluster complexed to two Na ions, and a dimer of ASA complexed to $K^+$.

### 3.1. Effect of additives

Salt additives, such as sodium trifluoroacetate (NaTFA), are sometimes critical to the success of MALDI experiments such as those conducted on synthetic polymers lacking hydroxyl and amino functional groups [20]. Studies suggest that cationized molecules in MALDI are generated by ion–molecule reactions in the gas phase [21].

MALDI mass spectra recorded in this work using a 1:3 ASA:DHB matrix and a 2:6:1 ASA:DHB:NaTFA matrix, are shown in Fig. 3. Although some features were enhanced by the addition of the salt, overall there is relatively little difference in the intensity of the $(ASA + Na)^+$ peak at $m/z = 203$. This is likely because the concentration of sodium impurities in the sample was already sufficiently large that the addition of more $Na^+$ made no real difference.

Performing the same experiment but using the same amount of potassium chloride (KCl) instead of NaTFA resulted in the near suppression of the $(ASA + Na)^+$ and $(ASA - H + 2Na)^+$ peaks, as well background peaks due to the matrix. As shown in Fig. 4c the resultant MALDI mass spectrum is now dominated by a feature which is assigned to $(ASA - H + 2K)^+$. Similarly, the addition of rubidium chloride (RbCl), or the addition of cesium chloride (CsCl), also resulted in the suppression of the sodiated

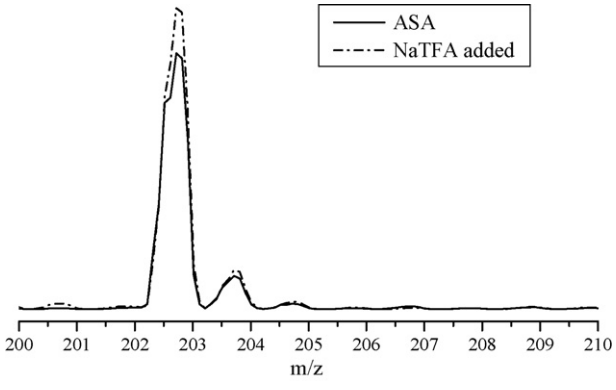


Fig. 3. A comparison of the MALDI $[ASA + Na]^+$ peak at $m/z = 203$, obtained by adding sodium triflouroacetate (NatFA) to that obtained without the salt additive.

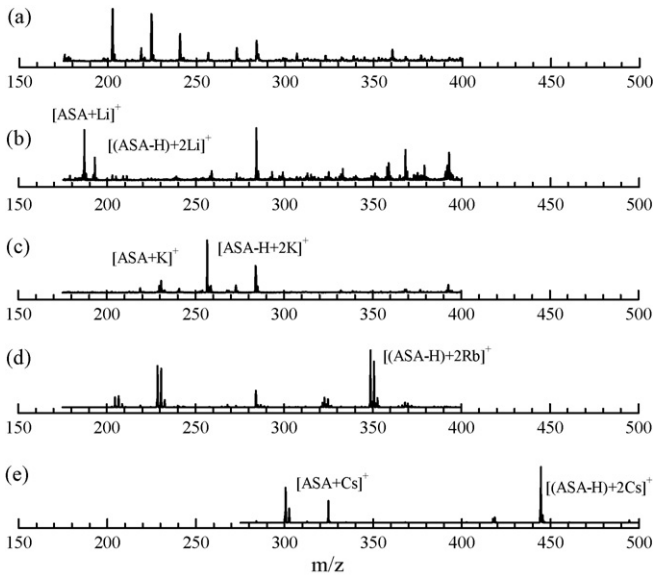


Fig. 4. MALDI mass spectra of (a) aspirin without additive, and those recorded with the addition of (b) LiCl, (c) KCl, (d) RbCl and (e) CsCl.

peaks, with the resultant mass spectra (Fig. 4d and e, respectively) dominated by a signal corresponding to deprotonated aspirin adduct containing two metal ions. While the addition of LiCl also suppressed the signals from the sodiated aspirin, the spectrum (Fig. 4b) is noisier and the strongest feature corresponds to the aspirin adduct containing a single Li ion.

It should be noted that cationization with the heavier alkalis not only yields cleaner spectra but it also shifts the main aspirin features into a mass region where matrix interference is less likely. The formation of $Rb_2Cl^+$ and $Cs_2Cl^+$ is attributed to gas-phase reactions in the MALDI plume. Other peaks observed using RbCl and CsCl additives can be assigned deprotonated acetic acid with two alkali metals attached. Aspirin is known to react with water to form acetic acid and 2-hydroxybenzoic acid [22]. Water may be present from the solvents used to form the matrix and/or be a fragmentation product of DHB and/or aspirin in the MALDI plume.

The spectrum obtained by adding equimolar amounts of RbCl and CsCl to the DHB/ASA matrix can be inspected in Fig. 5. Again, the spectrum is dominated by deprotonated aspirin adducts containing two alkali metal atoms. The $Cs_2$ related peaks are stronger than those containing Rb suggesting that CsCl is a more effective cationization source.

The detection limit of 0.25 nmol found for ASA alone decreased an order of magnitude to 0.015 nmol with the addition of the Rb or Cs alkali salts. These results are still poor compared to the low picomole [23,24] and even femtomole [25] detection limits often seen for other analytes, which probably explains why there have been no reports of MALDI being used to detect this drug molecule. Although the proton affinity of aspirin ($\sim$868 kJ $mol^{-1}$ [26]) is slightly higher than that for DHB ($855 \pm 8$ kJ $mol^{-1}$ [27]) the uncertainty in these values make it difficult to know if the choice of matrix in this experiment was a factor. Still, it is clear that salt additives are helpful when using DHB.

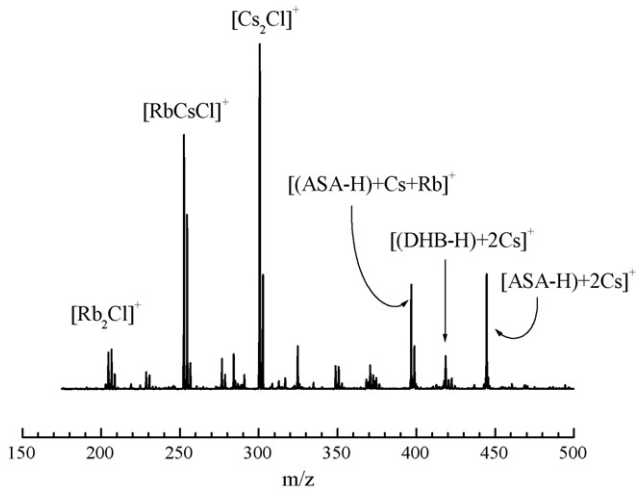


Fig. 5. MALDI mass spectrum obtained by adding equimolar amounts of RbCl and CsCl to an aspirin:DHB matrix.

While metal cationization in MALDI has been used for synthetic polymers [20,28], polystrenes [29], and oligo (*p*-phenyleneethynylene)s [30], there have been few systematic studies of its use with small drug molecules. In general, cations are known to bind strongly to aromatic systems [31]. Cation–π interactions for example are thought to be prominent in biological systems, where they can determine the structure of macromolecules.

Experimental evidence of a cation–π interaction between potassium ions and benzene in the gas phase was reported more than 20 years ago where the $K^+$–benzene binding energy was determined to be −19.2 kcal/mol [32]. For benzene, which is non-polar due to symmetry, the positive cation is electrostatically attracted to the quadrupole moment of benzene's π-system, and interacts along the ring's six-fold axis. A more recent calculation on the binding enthalpies for alkali–cation–benzene complexes reports binding energies of −20.1, −16.4 and −12.4 kcal/mol for the $K^+$, $Rb^+$ and $Cs^+$ complex, respectively [33]. The trend in the binding energy appears to reflect the decreasing positive surface charge density when going from $K^+$ to $Rb^+$. The Cs–aspirin complexes are the most intense features in the observed mass spectra, which appear to imply an opposite trend to that of the benzene-alkali system. Furthermore, except for the Li-adduct, aspirin appears to prefer binding two alkali metal ions.

### 3.2. Theoretical calculations

To understand these observations further, density functional theory (DFT) calculations were carried out to find the optimized structures of the aspirin–alkali metal ion complexes observed, and to establish the extent that cation–π interactions determine the binding energetic and geometries.

The global minimum energy structure of the aspirin molecule itself was found by initially performing a Monte-Carlo-based optimization scheme as implemented in the Spartan'02 package [34] at the PM3 semi-empirical level of theory [35]. The 12 lowest energies structures were selected, and their geometries optimized at the B3LYP/LACV3P (d,p) level of theory [36,37] with the Jaguar software package. The lowest energy structure was selected as the energetically preferred conformation of ASA, and used as the basis for further calculations.

The ASA molecule contains several sites which the alkali cations can coordinate to, including each oxygen atom, as well as both sides of the phenyl ring. Calculations were performed at the B3LYP/LACV3P (d,p) level of theory to determine the preferred coordination site and the molecular geometry of $(ASA - M)^+$ adducts. In this series of calculations, $M^+$ was coordinated to one of the sites (on one side or the other side of the phenyl ring, or the four sites associated with the oxygen atoms), for a total of six initial structures. The lowest energy results show that each alkali metal cation prefers to coordinate with the carboxylic acid and ester groups to form an eight member ring (Fig. 6).

DFT was then used to determine the minimum energy structures of the deprotonated aspirin containing two alkali metal ions $(ASA - H + 2M)^+$. A broader global geometry optimization scheme was employed here due to the increased structural complexity, and the potential for structural diversity of the $(ASA - H + 2M)^+$ ions. The first step in the calculation involved

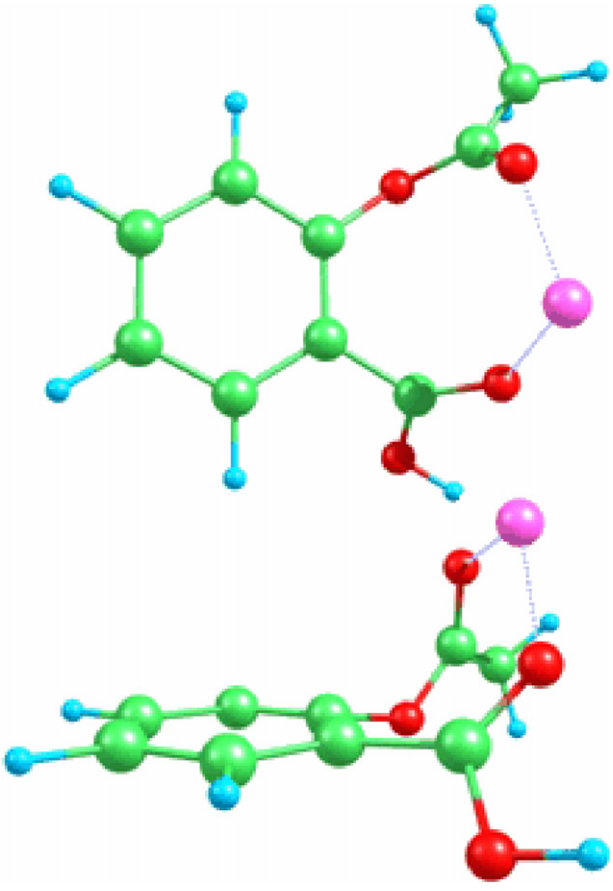

Fig. 6. Optimized top and side view structures determined by DFT for the $[ASA + M]^+$ cation for M = Li, Na, K, Rb and Cs. Carbon atoms are shown in green, oxygen atoms in red, hydrogen atoms in blue, and the alkali cation in purple. While the basic geometries of the adducts are similar there are differences in the $M^+$-ASA bond lengths and angles. (For interpretation of the references to color in this figure legend, the reader is referred to the web version of the article.)

generating structures for $(ASA - H + 2M)^+$ by removing the hydrogen atom from the acid O–H bond in $(ASA - M)^+$, and then adding a second cation to one of the possible coordination sites. A total of 10 bonding configurations for each dication adduct was considered in this work. A 1.0 ns molecular dynamics (MD) simulations was performed at 1000 K using the Universal 1.02 force-field [38] as implemented in the Cerius2 molecular modeling package [39]. Since force-field-based simulations do not allow for bond formation or dissociation, the chosen bonding configuration was maintained throughout the simulation; that is, the cations remained at the sites to which they were assigned. The temperature chosen for the simulations was sufficiently high to allow the system to sample a large number of configurations.

In the second step of the optimization scheme, hundreds of configurations were sampled at regular intervals and optimized at the HF/LANLMB level of theory with the Gaussian98 suite of programs [40]. The 20 lowest energy structures were then optimized with Jaguar at the B3LYP level of DFT using a 3-21G(d) basis set used on C, O and H, and a LACV3P(d) basis on the cations. The 10 lowest energy structures from this procedure were further optimized at the B3LYP/LACV3P (d,p) level of theory with Jaguar, and the lowest energy structure was identified as the preferred geometry of the dication. It should be noted that in this global optimization scheme, a total of 1000 initial structures were sampled and filtered down to a single minimum energy structure for each cation considered in this work. Although, this does not guarantee that global minima were found, it does represent a substantial exploration of the conformational space.

The three lowest energy structures determined for the $Li^+$, $Na^+$, $K^+$, $Rb^+$ and $Cs^+$ di-substituted species are shown in Fig. 7a–e. In each case one of the alkali cations is located between the two carbonyl oxygens belonging to the acid and ester groups, while the second cation is more closely associated with the oxygens on the acid group. Except for Li species there is also some interaction between the second alkali cation and the phenyl-π system. However, in no case does an alkali metal sit directly above the phenyl ring.

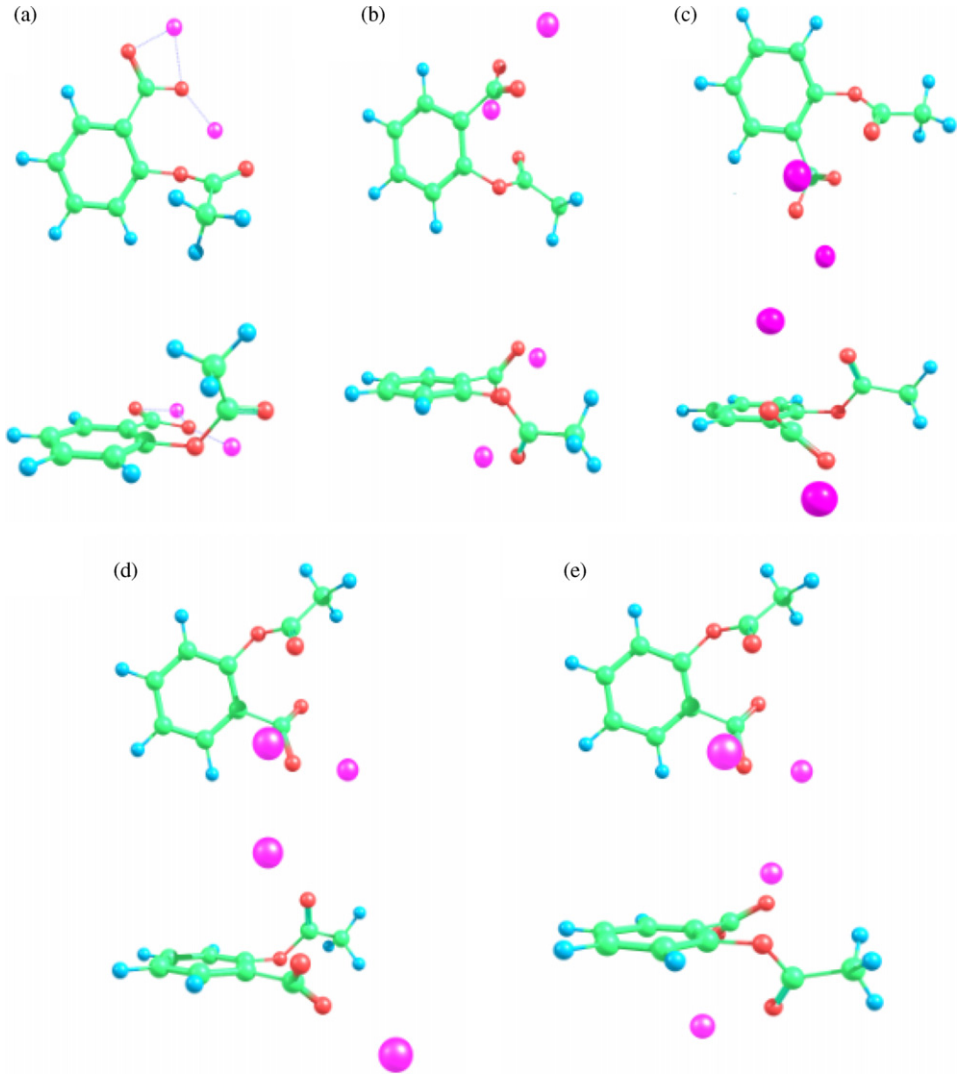


Fig. 7. Optimized top and side view structures determined by DFT calculations for (a) $[(ASA - H) + 2\ Li]^+$, (b) $[(ASA - H) + 2Na]^+$, (c) $[(ASA - H) + 2K]^+$, (d) $[(ASA - H) + 2Rb]^+$ and (e) $[(ASA - H) + 2Cs]^+$. Carbon atoms are shown in green, oxygen atoms in red, hydrogen atoms in blue, and the alkali cations in purple. (For interpretation of the references to color in this figure legend, the reader is referred to the web version of the article.)

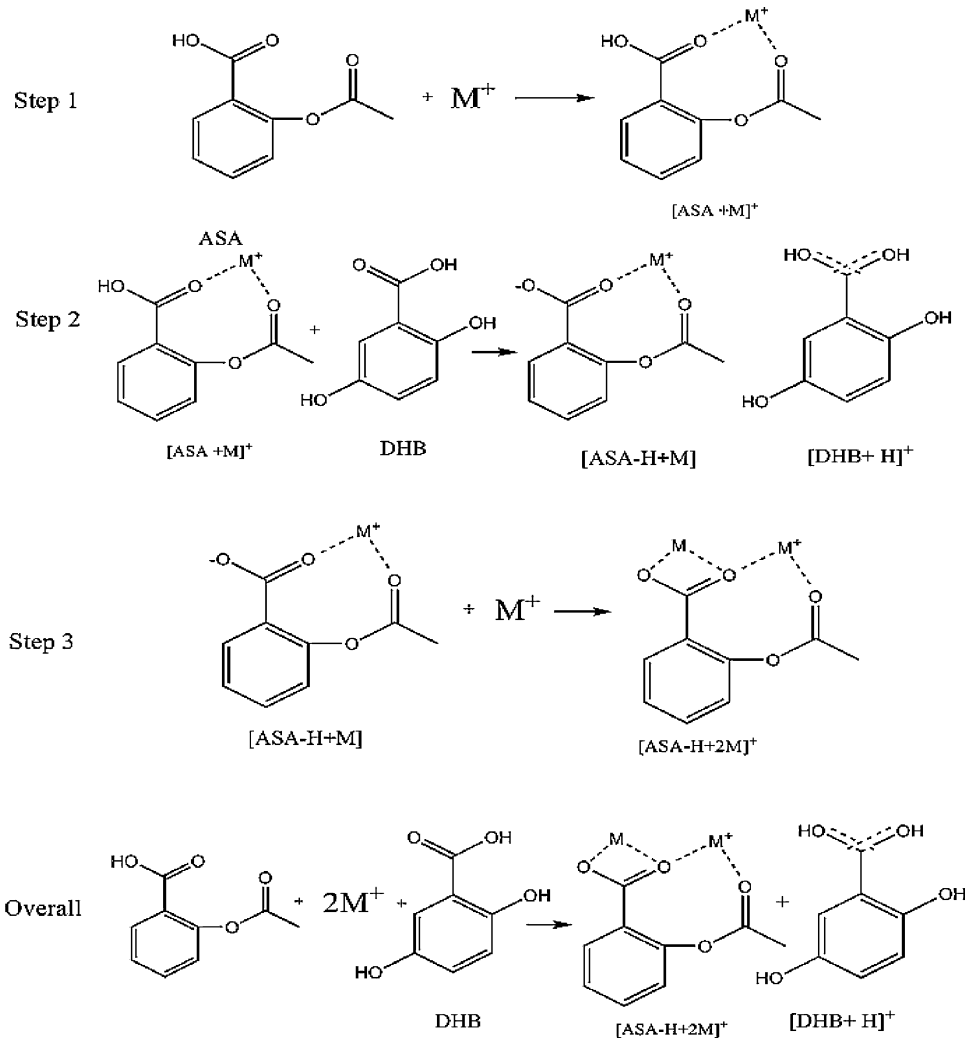


Fig. 8. Mechanism used to calculate the energetics of alkali metal ion—aspirin adduct formation.

The reaction energies were evaluated for the stepwise addition of alkali cations to the ASA molecule through the mechanism outlined in Fig. 8. In the first step, a cation (M) coordinates to the oxygen atoms in the carbonyl groups of the ASA molecule. In the second step, the $(ASA - M)^+$ complex loses a proton to DHB to form $(ASA - H + M)$ and $(DHB\text{-}H)^+$. In the third step, a second cation reacts with $(ASA - H + M)$ to form $(ASA - H + 2M)^+$. The associated reaction energies for each of these steps are given in Table 2. The energetics for the overall reaction $ASA + 2M^+ \rightarrow (ASA - H + 2M)^+ + H^+$ are also given in that table. The overall reaction is exothermic for all of the alkali cations considered in the calculations.

Table 2
Reaction energies[a] (kcal/mol) for the individual steps shown in Fig. 8, as well as the overall reaction energy for the full reaction of ASA with $2M^+$ in the presence of DHB

| Step 1 | | Step 2 | | Step 3 | | Overall[a] | |
|---|---|---|---|---|---|---|---|
| M | $\Delta E$ | M | $\Delta E$ | M | $\Delta E$ | M | $\Delta E$[b] |
| Li | −68.9 | Li | 34.2 | Li | −75.5 | Li | −110.3 |
| Na | −48.1 | Na | 38.2 | Na | −59.1 | Na | −69.0 |
| K | −26.3 | K | 46.3 | K | −51.2 | K | −35.4 |
| Rb | −25.9 | Rb | 49.2 | Rb | −40.7 | Rb | −17.3 |
| Cs | −21.6 | Cs | 52.7 | Cs | −37.0 | Cs | −5.9 |

[a] Energy for the total reaction $ASA + 2M^+ + DHB \rightarrow (ASA - H + 2M)^+ + (DHB + H)^+$.
[b] Electronic energies calculated at the B3LYP/LACV3P (d,p) level of theory.

The trend in the overall reaction energies given in Table 2 shows that the products of the reaction become less exothermic as the size of the alkali cation increases. The stabilities of the adducts are governed by various factors including the strength with which the cation binds to the oxygen atoms and the π-system in ASA, as well as the energetic penalty associated with the distortion of the ASA moiety from is preferred molecular geometry to that in the $(ASA - H + 2M)^+$ complex.

## 4. Discussion and conclusions

The results of the calculations above can be compared to a recent DFT study on alkali cation interactions with the aromatic amino acid, phenylalanine. Here, the cation–π binding modes were found to be competitive with non-π binding modes. Specifically, the alkali metal cations were found to bind in a tridentate mode to the carbonyl oxygen and amino nitrogen,

while the cation–π interaction provided extra stabilization because the metal ion sits above the center of the phenyl ring [41]. The trends calculated also indicate that the binding affinities of the phenylalanine–alkali adducts decreases in the order $Li^+ < Na^+ < K^+$, mimicking the benzene–alkali metal ion case.

One possible simple explanation that can account for the discrepancy between theory and experiment is the energetics and mechanism of alkali cation formation. Although it is difficult to know the extent of dielectric screening in the matrix phase [42], one can consider the energies of the reaction $MCl(s) \rightarrow M^+(g) + Cl^-(g)$ as a metric of the ease of alkali cation formation. These values decrease going from Li to Cs [43]. The melting and boiling point of the alkali chlorides also decrease going from Li to Cs, although KCl sublimes rather than boils. If the DHB molecule is the main constituent in the matrix that absorbs the $N_2$ laser light, then these trends suggest that the net energy available to form $M^+$ after plume formation would favor the formation of $Cs^+ > Rb^+ > K^+ > Na^+ > Li^+$. This would also not only explain the intensity effects as a function of alkali salt but also why the mono-lithiated adduct is more abundant than the dication species.

## Acknowledgements

This work was supported by the Natural Sciences and Engineering Research Council of Canada (NSERC). The authors from Western are grateful to MDS-Sciex for their generous in-kind donation of the MALDI mass spectrometer to their lab.

## References

[1] J.R. Vane, R.M. Botting (Eds.), Aspirin and Other Salicylates, Chapman & Hall, London, 1992.
[2] E.H. Awtry, J. Loscalzo, Circulation 101 (2000) 1206.
[3] R.S. Sandler, S. Halabi, J.A. Baron, Cancer Treat. Rev. 29 (2003) 329.
[4] T. Philips, C. Leeuwenburgh, Rejuvenation Res. 7 (2004) 243.
[5] L. Macchi, N. Sorel, L. Christiaens, Curr. Pharmaceut. Des. 12 (2006) 251.
[6] H. Chen, N.N. Talaty, Z. Takáts, R.G. Cooks, Anal. Chem. 77 (2005) 6915.
[7] Y. Cai, D. Kingery, O. McConnell, A.C. Bach II, Rapid Commun. Mass Spectrom. 19 (2005) 1717.
[8] D. Tsikas, K.S. Tewes, F.-M. Gutzki, E. Schwedhelm, J. Greipel, J.C. Frölich, J. Chromatogr. B 709 (1998) 79.
[9] G.P. McMahon, M.T. Kelly, Anal. Chem. 70 (1998) 409.
[10] M. Karas, F. Hillekamp, Anal. Chem. 60 (1988) 2299.
[11] L.H. Cohen, A.I. Gusev, Anal. Bioanal. Chem. 373 (2002) 571.
[12] A. Tholey, C. Wittman, M.-N. Kang, D. Bungert, K. Hollemeyer, E. Heinzle, J. Mass Spectrom. 37 (2002) 963.
[13] Z. Guo, Q. Zhang, H. Zou, B. Guo, J. Ni, Anal. Chem. 74 (2002) 1637.
[14] P. Hatsis, S. Brombacher, J. Corr, P. Kovarik, D.A. Volmer, Rapid Commun. Mass Spectrom. 17 (2003) 2303.
[15] J. Gobey, M. Cole, J. Janiszewski, T. Covey, T. Chau, P. Kovarik, J. Corr, Anal. Chem. 77 (2005) 5643.
[16] L. Sleno, D.A. Volmer, Anal. Chem. 77 (2005) 1509.
[17] L. Sleno, D.A. Volmer, Rapid Commun. Mass Spectrom. 19 (2005) 1928.
[18] L. Li, R.E. Golding, R.M. Whittal, J. Am. Chem. Soc. 118 (1996) 11662.
[19] G. McCombie, R. Knochenmuss, Anal. Chem. 76 (2004) 4990.
[20] M.W.F. Nielen, Mass Spectrom. Rev. 18 (1999) 309.
[21] B.H. Wang, K. Dreisewerd, U. Bahr, M. Karas, F. Hillenkamp, J. Am. Soc. Mass Spectrom. 4 (1993) 393.
[22] L. Nelander, Acta Chem. Scand. 18 (1964) 973.
[23] P.K. Salo, H. Salomies, K. Harju, R.A. Ketola, T. Kotiaho, J. Yli-Kauhaluoma, R. Kostiainen, J. Am. Soc. Mass Spectrom. 16 (2005) 906.
[24] P.J. Lee, W. Chen, J.C. Gebler, Anal. Chem. 76 (2004) 4888.
[25] J. Falkenhagen, S.M. Weidner, Rapid Commun. Mass Spectrom. 19 (2005) 3724.
[26] R.R. Kunz, W.F. Dinatale, P. Becotte-Haigh, Int. J. Mass Spectrom. 226 (2003) 379.
[27] F.H. Yassin, D.S. Marynick, Mol. Phys. 103 (2005) 183.
[28] G. Montaudo, F. Samperi, M.S. Montaudo, Prog. Polym. Sci. 31 (2006) 277.
[29] H. Rashidezadeh, B. Guo, J. Am. Soc. Mass Spectrom. 9 (1998) 724.
[30] H. Chen, M. He, Z.-K. Chen, C.-Z. Zhou, J. Am. Soc. Mass Spectrom. 16 (2005) 1695.
[31] J.C. Ma, D.A. Dougherty, Chem. Rev. 97 (1997) 1303.
[32] J. Sunner, K. Nishizawa, P. Kebarle, J. Phys. Chem. 85 (1991) 1814.
[33] D. Feller, D.A. Dixon, J.B. Nicholas, J. Phys. Chem. A 104 (2000) 11414.
[34] Spartan'02, Wavefunction Inc., Irvine, CA, 2002.
[35] J.J.P. Stewart, J. Comp. Chem. 10 (1989) 209.
[36] The LACV3P basis set uses a 6-311G basis set on C, O, H, Li and Na, and effective core potentials on K, Rb and Cs. The label (d,p) indicates the addition of polarization functions on all atoms.
[37] A.D. Becke, J. Chem. Phys. 98 (1993) 5648.
[38] A.K. Rappé, K.S. Colwell, C.J. Casewit, Inorg. Chem. 32 (1993) 3438.
[39] Cerius2_4.2 Modeling Environment, Molecular Simulations Inc., San Diego, 1999.
[40] M.J. Frisch, G.W. Trucks, H.B. Schegel, G.E. Scuseria, M.A. Robb, J.R. Cheeseman, V.G. Zakrewski, J.J.A. Montgomery, R.E. Stratmann, J.C. Burant, S. Dapprich, J.M. Millam, A.D. Daniels, K.N. Kudin, M.C. Strain, O. Farkas, J. Tomasi, V. Barone, M. Cossi, R. Cammi, B. Mennucci, C. Pomelli, C. Adamo, S. Clifford, J. Ochterski, G.A. Petersson, P.Y. Ayala, Q. Cui, K. Morokuma, D.K. Malick, A.D. Rabuck, K. Raghavachari, J.B. Foresman, J. Cioslowski, J.V. Ortiz, A.G. Baboul, B.B. Stefanov, G. Liu, A. Liashenko, P. Piskorz, I. Komaromi, R. Comperts, R.L. Martin, D.J. Fox, T. Keith, M.A. Al-Laham, C.Y. Peng, A. Nanayakkara, C. Gonzalez, M. Challacombe, P.M.W. Gill, B.G. Johnson, W. Chen, M.W. Wong, J.L. Andres, M. Head-Gordon, E.S. Replogle, J.A. Pople, Gaussian 98 (Revision A.9), Gaussian, Inc., Pittsburgh, PA, 1998.
[41] F.M. Siu, N.L. Ma, C.W. Tsang, Chem. Eur. J. 10 (2004) 1966.
[42] R. Zenobi, R. Knochenmuss, Mass Spectrom. Rev. 17 (1998) 337.
[43] G. Che, R.G. Cooks, J. Mass Spectrom. 32 (1997) 1258;
C.K. Kim, J. Won, H.S. Kim, Y.S. Kang, H.G. Li, C.K. Kim, J. Comput. Chem. 22 (2001) 827;
L. Wu, J.W. Denault, R.G. Cooks, L. Drahos, K. Vékey, Am. Soc. Mass Spectrom. 13 (2002) 1388.